

Topological Solitons in Chiral Nematic Liquid Crystals

Final Report

Ramin Tawab

Department of Physics, University of Warwick, Coventry CV4 7AL, United Kingdom

Topological solitons are particle-like objects that are encoded in the field lines of various physical systems. Recent experiments with chiral nematic liquid crystals have generated a new class of topological solitons that have not previously appeared in the theoretical literature. We use the solid angle function to construct a unified model of all ordinary topological solitons and then extend it to this new class. Our approach is shown to supersede the well established rational map construction. The chiral energy of a system is introduced and used to quantify the stability of these objects in a setting that is divorced from any specific field theory. This is supplemented by numerical minimisation of the free energy. These results formalise the relationship between the stability, chirality and dynamics of soliton field configurations and therefore are of consequence to several branches of physics.

I. Introduction

Topological solitons are localised regions of a physical field with a knotted structure which means that they cannot be annihilated through continuous deformations [1]. Their particle-like nature led Lord Kelvin to choose them as an early candidate for the atom [2]. They appear in diverse areas of modern physics including theories of electromagnetism [3], fluids [4], plasmas [5], gravitation [6], elementary particles [1], and early universe cosmology [7]. They show promise in applications to nano-electronics [8], self-healing materials [9], bi-stable displays [10], photonic devices [11], and novel forms of computer memory that exploit their topological charge [12].

Theoretically, these objects are described using homotopy theory which classifies different textures by their ability to continuously deform [13]. In particular, the mathematical Hopf map demonstrates how to fill space with interlinked loops and generates a group of three-dimensional topological solitons known as Hopfions [14]. The Hopf map also appears in several areas of physics and the study of its properties is of great importance [15]. While three-dimensional topological solitons have not been reliably observed in most physical systems, they are a key feature of many theories [16]. However, recent breakthroughs have allowed for the experimental creation of Hopfions, Torons, Twistions and other three-dimensional topological solitons in cholesteric liquid crystals [14, 17]. These objects have also been successfully arranged into grids that fill space, thus paving the way for the discovery of novel phases of condensed matter [18].

Historically, experimental breakthroughs of this nature have elucidated the theoretical understanding of topological solitons [19]. Furthermore, the naive application of mathematical theory has on occasion been contradicted by subsequent experiments with liquid crystals [20]. Therefore, it is crucial for us to investigate Hopfions and other topological solitons in the context of liquid crystals for which detailed experiments exist. Specifically, we will study the topological and energetic properties of these observed structures and generalise them to more complicated textures with higher topological charge that have not yet been observed, so as to pave the way for further experiments.

A. Liquid Crystals

Liquid crystals are phases of matter that lie between simple liquids and traditional crystals in their molecular order [21]. In particular, they possess the positional disorder of liquids which manifests in their ability to flow while also exhibiting the anisotropy of crystals which leads to interesting properties in their response to light and electromagnetic fields. We will consider thermotropic liquid crystals which are composed of rod-shaped molecules (see figure 1a) whose order is understood in terms of both their orientation and position.

Formally, the orientational order of a liquid crystal composed of rod-shaped molecules with long axis \mathbf{u} at a point \mathbf{x} can be described through the traceless and symmetric tensor

$$Q_{ij}(\mathbf{x}) = \langle u_i u_j - \frac{1}{3} \delta_{ij} \rangle,$$

where the average is over all molecules in an infinitesimal neighbourhood of \mathbf{x} . For a uniaxial system, this tensor can be written in terms of its principal eigenvalue S and

corresponding eigenvector \mathbf{n} [22]. Then

$$Q_{ij} = S(n_i n_j - \frac{1}{3} \delta_{ij}).$$

Physically, \mathbf{n} describes the average preferred orientation of the medium and is known as the director of the liquid crystal [23]. Since its constituent molecules are non-polar, the orientations \mathbf{n} and $-\mathbf{n}$ are equivalent. On the other hand, S describes the strength with which the molecules are oriented along this director and is known as the scalar order parameter.

The nematic phase has a uniform director throughout the material but lacks positional ordering among its molecules (see figure 1a). In contrast, chiral nematics have a helical director which is said to be chiral since it is asymmetric with respect to its mirror image. The distance over which the director performs a full rotation is the pitch p . Chiral nematics may be schematised as a twisted nematic phase and nematics can be thought of as chiral nematics with infinite pitch. The chiral mesophase was first observed in cholesteryl compounds and is thus also known as the cholesteric phase [24]. However, it is more readily obtained from ordinary nematics by introducing small amounts of a chiral dopant molecule.

The director of a liquid crystal can be imaged through polarising microscopy [24]. The liquid crystal is placed between two linear polarisers with their transmission axes oriented at right angles to each other. Since nematics are birefringent, the electric field components of light parallel and normal to the director experience different refractive indices [25]. The resulting phase difference causes the transmitted light to become elliptically polarised. Thus, some component of the light passes through the second polariser. The light is blocked whenever the director is parallel to the polarisation axis of either polariser or if the liquid crystal transitions to an isotropic phase. Similar techniques can be used to image other mesophases as well as three dimensional liquid crystals [14].

The resulting textures map orientations to colours and can be viewed as preimages of the director field (see figure 1b). They show that real liquid crystals deviate from the uniformity of figure 1a. Indeed, the boundary conditions of the material may induce three independent types of elastic distortions which continuously deform the director field [21]. The cost that these incur on the liquid crystal is defined by the Frank free energy

$$F = \int_V dV \left\{ \frac{1}{2} K_1 (\nabla \cdot \mathbf{n})^2 + \frac{1}{2} K_2 (\mathbf{n} \cdot \nabla \times \mathbf{n} + q_0)^2 + \frac{1}{2} K_3 (\mathbf{n} \times \nabla \times \mathbf{n})^2 \right\}, \quad (1)$$

where K_1 , K_2 , and K_3 are positive constants corresponding to the bend, twist, and splay distortions respectively (see figure 1c). For a cholesteric liquid crystal, the chirality q_0 assumes a non-zero value equal to $2\pi/p$ where p is the pitch. Further coupling terms may be introduced to the free energy in the presence of an external electromagnetic field.

To determine stable director field configurations, it is sufficient to minimise this free energy [21]. This can be done through a numerical relaxation algorithm that iteratively constructs a minimised director field given an initial configuration [14]. Thus, experimental realisations of stable topological solitons can be supplemented by a numerical minimisation of the free energy where the initial conditions approximate those of the experiment.

In addition to this, liquid crystals respond to electromagnetic fields. While their constituent molecules are dielectric and diamagnetic, it is the collective orientational order of liquid crystals that amplifies the effects of an external field on the medium [21]. When the applied field surpasses a critical value, the director field aligns with the external field through a continuous Fréedericksz transition [23]. This effect allows one to manipulate the director field using laser tweezers and can be used to tie lines of constant orientation in the director field together to form various topological solitons [14].

B. Topological Solitons

Since the director indicates an orientation in \mathbb{R}^3 without specifying a direction, it can be schematised as a member of the real projective plane, \mathbb{RP}^2 . This is the set of all lines through the origin in \mathbb{R}^3 and can be visualised as a sphere with the understanding that antipodal points are equivalent (see figure 2a). Hence, the texture of a liquid crystal forms a line field.

Two director field configurations are said to be homotopic if they can be continuously distorted to look like each other. Formally, continuous director fields $\mathbf{n}_1, \mathbf{n}_2 : \mathbb{R}^3 \rightarrow \mathbb{RP}^2$ are homotopic if there exists a continuous function $H : \mathbb{R}^3 \times [0, 1] \rightarrow \mathbb{RP}^2$ such that $H(\mathbf{x}, 0) = \mathbf{n}_1(\mathbf{x})$ and $H(\mathbf{x}, 1) = \mathbf{n}_2(\mathbf{x})$ [13]. If they are homotopic, they are said to belong to the same homotopy class. If they are not homotopic, there is a non-negligible energy barrier forbidding the transition from \mathbf{n}_1 to \mathbf{n}_2 [26]. In this way, localised non-trivial director field configurations can exist that remain stable due to their topological properties. These are known as topological solitons.

Perhaps the simplest such example is the hedgehog. This is a point singularity from

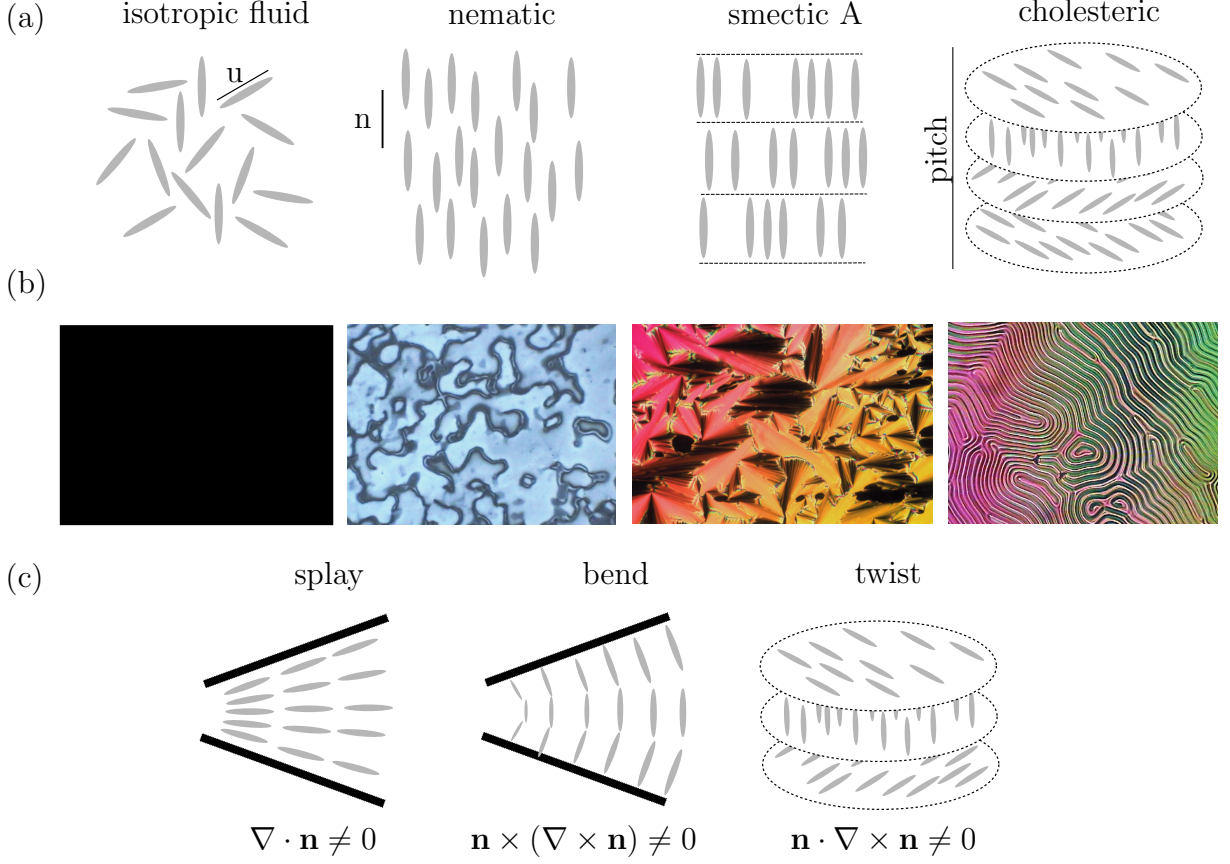


Figure 1: (a) Schematic of the isotropic liquid phase, and the nematic, smectic A, and cholesteric liquid crystal mesophases. The orientation \mathbf{u} , director \mathbf{n} , and pitch p are shown. (b) The texture of an isotropic liquid is black; the nematic phase may appear uniform with thread-like disclination lines where the director is in the direction of light propagation; the smectic A phase may appear fan-shaped with the layers of uniform director clearly separated; cholesteric liquid crystals may exhibit a fingerprint texture where the distance between two dark stripes is half the pitch. Images reproduced from [24]. (c) Schematic of the splay, bend, and twist director distortions with corresponding non-zero characteristic quantities.

which the director emanates radially outwards akin to $\mathbf{n}(\mathbf{x}) = \mathbf{x}/|\mathbf{x}|$ [27]. We can conceptually enclose such a hedgehog with a sphere, S^2 , and consider the director field along this sphere, $\tilde{\mathbf{n}} : S^2 \rightarrow \mathbb{R}P^2$. This allows one to classify the hedgehog by the degree of this map. The degree is an integer that describes how many times a point on $\mathbb{R}P^2$ is covered under $\tilde{\mathbf{n}}$ [28]. Since the degree is conserved between homotopic maps on spheres, we use it as a topological charge to characterise the homotopy classes of hedgehogs. Formally, we write $\pi_2(\mathbb{R}P^2) = \mathbb{Z}$ to state that there are an infinite number of homotopy classes of hedgehog induced maps $\tilde{\mathbf{n}}$ corresponding to an integer topological charge [13].

Hedgehogs are known as point defects because they introduce a point in the material where the director is undefined. However, we will focus on topological solitons that form continuous textures. To study these, we will need to map from \mathbb{R}^3 to the order parameter space $\mathbb{R}P^2$. We can view \mathbb{R}^3 as the sphere S^3 embedded in 4 dimensions using stereographic projection (see figure 2b). We choose a reference point N on the sphere and

associate each point P on $S^3 \setminus \{N\}$ with the unique point on \mathbb{R}^3 that intersects the line connecting N and P . We can associate N with infinity since these textures are localised and the director is assumed to be uniform in the far field. An advantage of stereographic projection is that it is a conformal map [29] and thus preserves angles at which curves meet and is therefore suited to studying the orientation of the director field.

Consequently, we can study smooth three dimensional liquid crystal textures as elements of $\pi_3(\mathbb{RP}^2)$. This is the homotopy group of continuous maps $\mathbf{n} : S^3 \rightarrow \mathbb{RP}^2$, an explicit example of which is given by the standard Hopf map introduced in section II A.

The homotopy classes of such maps are classified by their integer Hopf invariant [1]. Geometrically, the Hopf invariant is given by the linking number of the preimages of any two distinct regular values of f . The standard Hopf map has Hopf invariant 1. Indeed, the preimage of a pair of distinct points under the Hopf map is a pair of linked loops with linking number 1. Thus, the Hopf invariant can also be defined as the number of times that f sweeps S^2 when traversing S^3 [14].

In figure 1b, we illustrated planar director fields by assigning each orientation a different colour. This can be extended to three dimensions through the Pontryagin–Thom (PT) construction [27, 28]. We consider preimages of the equator on \mathbb{RP}^2 and colour points by their azimuthal orientation. Figure 2d shows a PT rendering of the Hopf map. Figure 2e shows a PT rendering of an experimentally constructed director field configuration observed in a cholesteric liquid crystal. Incredibly, these constructions are homotopic and the latter is an experimental realisation of a topological soliton appropriately named the Hopfion. The characteristic linking of preimages of this soliton is shown in figure 2f.

Since these structures are axisymmetric, we classify them by the amount of twist they introduce in any radial direction. For example, the standard Hopf map introduces a full 2π twist in radial directions as can be seen by the full colour winding in its PT construction. As more twisting is embedded, the linking of preimages has shown to adopt a non-uniform characterisation that can no longer be determined through the simple linking number of a pair of points as was the case for the mathematical Hopf map (see figure 2i). In fact, the twisting of the director field within these solitons also exhibits a non-uniformity which potentially helps to stabilise the soliton [14].

We can construct a map with arbitrary Hopf invariant k by composing the Hopf map η with a degree k map [13]. However, it is often possible to form geometrically distinct links that have the same linking number (see figure 2c). These are nonetheless link homotopic and can be distorted to look like each other assuming that each constituent knot is allowed

to pass through itself [30]. It is challenging then to construct a map with its preimages linking in all such possible manners.

To further complicate matters, it is possible for otherwise smooth solitons to feature point or line defects. One such example is the Toron (see figure 2g). This is a twisted region of director field that is flanked by hyperbolic hedgehogs which allow it to be embedded into a uniform background. Twistions also exist (see figure 2h) which are asymmetric regions of twisted director that contain multiple point defects. Evidently, the mathematical description of such objects is complicated by the diversity of their topological, geometric, and energetic properties. We will therefore attempt to provide a systematic classification of these matters.

II. Theoretical Details

Topological solitons are commonly described using rational maps. Herein an alternative approach is introduced using the solid angle function and it is shown to be complementary to the well established rational map construction.

A. Rational Map Construction

The standard Hopf map can be written as

$$\eta : \mathbb{C}^2 \rightarrow \hat{\mathbb{C}}, \quad \eta(z_1, z_2) = \frac{z_1}{z_2}. \quad (2)$$

The domain of the map is all pairs of complex numbers such that the sum of their magnitudes is unity. This can be identified with the sphere S^3 . The co-domain of the map is the set of complex numbers with an additional point at infinity and may be viewed as the sphere S^2 via inverse stereographic projection (see figure 2b). Strictly speaking, this is a map from S^3 to S^2 but has many of the same properties as a map onto \mathbb{RP}^2 .

The construction of the standard Hopf map in (2) can now be extended to generate further knotted fields by considering rational maps

$$\psi : \mathbb{C}^2 \rightarrow \hat{\mathbb{C}}, \quad \psi = \frac{p(z_1, \bar{z}_1, z_2, \bar{z}_2)}{q(z_1, \bar{z}_1, z_2, \bar{z}_2)},$$

where p and q are polynomials of two complex variables and their conjugates [31].

The Hopf invariant of such a map can be rigorously formulated using differential geometry [32, 33]. However, it is illustrous to restate this in terms of vector fields. Given

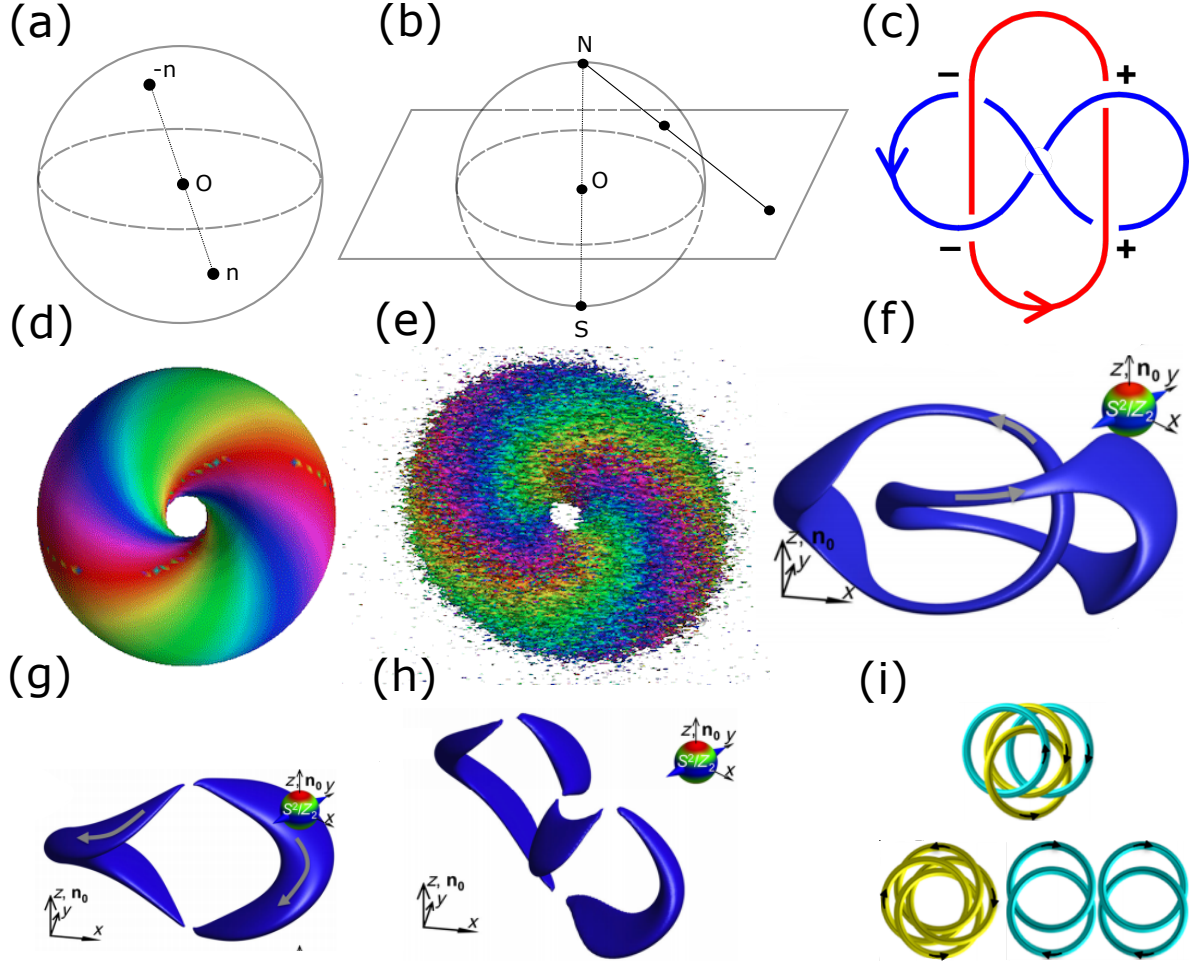


Figure 2: (a) \mathbb{RP}^2 can be visualised as S^2 with the equivalence $\mathbf{n} \equiv -\mathbf{n}$. (b) Stereographic projection of S^2 onto \mathbb{R}^2 . (c) The Whitehead link has linking number zero. This can be seen through a signed count of link crossings. Note that a pair of unlinked loops also have zero linking number. In fact, if we push the blue knot through itself, the links become disentangled. (d) The Hopf map visualised via the PT construction and (e) an experimental Hopfion imaged via the PT construction. Reproduced from [17]. (f) The preimage of a pair of antipodal points in S^2 (i.e. a point on \mathbb{RP}^2) forms a pair of closed loops. The consistent directions of circulation are indicated. (g) The preimage of an orientation in a Toron and (h) a Twiston. (i) The linking of preimages of a Hopfion with greater twist than 2π exhibits non-uniform linking throughout the soliton. Nonetheless, the Hopf invariant is conserved. Reproduced from [14]

a divergence free vector field \mathbf{B} that is everywhere tangential to ψ , there exists a vector potential \mathbf{A} such that $\mathbf{B} = \nabla \times \mathbf{A}$. Then the Hopf invariant of ψ is given by

$$h(\psi) = \int_{\mathbb{R}^3} \mathbf{A} \cdot \mathbf{B}$$

up to a singular Gauge transformation [31]. Geometrically, this coincides with the definition given in section I. A. as the linking number of the preimages of two distinct regular values of ψ . Thus, the Hopf invariant of a vector field may be defined as the helicity of its vector potential which must adopt an integer value. In particular, the helicity of the vector potential of a Hopfion is unity since $h(\eta) = 1$.

The advantage of this method is that it yields a closed form expression for a multitude of knotted field configurations. Furthermore, it provides an analytical means of evaluating the Hopf invariant. However, there is no known analytical method of deriving the rational map corresponding to a given field configuration and since the method restricts itself to only using rational maps, there are field configurations which it cannot describe.

B. Solid Angle Construction

The solid angle function has recently been used to model magnetic scroll waves and disclination lines in nematic liquid crystals [34]. The solid angle function ω of a curve K at a point \mathbf{x} may be viewed as the surface area enclosed by the projection of K onto the unit sphere centered at \mathbf{x} (see figure 3a). This is well defined on the complement of K . Furthermore, the solid angle is a harmonic function that satisfies Laplace's equation

$$\nabla^2 \omega = 0.$$

We may therefore view the solid angle of a curve K as the magnetic scalar potential of a wire in the shape of K that carries unit current. In particular, we can correspond this with the aforementioned magnetic vector potential \mathbf{A} via

$$\nabla \omega = \nabla \times \mathbf{A}.$$

Additionally, ω winds by 4π around the curve K (see figure 3b) and the surfaces of constant ω bunch along the curve normal in the far field (see figure 3c). Thus, the structure of ω in a tubular neighbourhood of the curve has both longitudinal and transverse components which may be used to construct a knotted field configuration using a parametric approach as shown in section III. C.

The advantage of this method is that it can be used to intuitively construct knotted field configurations by considering the behaviour of the field. Furthermore, the solid angle function is well defined for any curve K and is easily computed using numerical methods described in [34]. However, it fails to give a closed form expression due to the dependence on the solid angle which can only be written exactly in special cases such as for a circle where it is an infinite series of spherical harmonics [35].

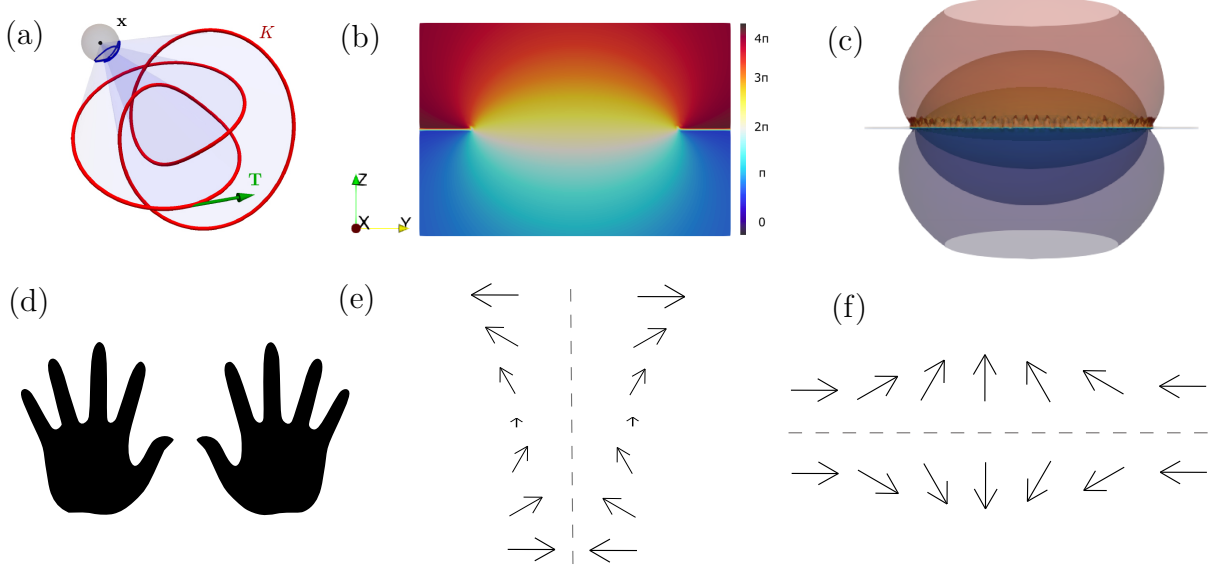


Figure 3: (a) The solid angle of a curve K evaluated at \mathbf{x} equals the surface area enclosed by its projection onto the unit sphere centered at \mathbf{x} . Reproduced from [34]. (b) A cross section of the solid angle of the unit circle in the xy -plane centered at the origin viewed from the direction normal to the zy -plane. The solid angle winds by 4π about the two points where the circle intersects the plane. (c) Isosurfaces of the solid angle of the same circle are shown. Surfaces of constant solid angle bunch up in the direction normal to the circle. (d) Human hands are intrinsically chiral. They cannot be superimposed on each other unless one of them is reflected. (e) This vector field behaves like a helix. As a particle is translated vertically, it rotates about the vertical axis. Its reflection is also shown and rotates with opposing handedness. This vector field is described by a diagonal element of the chirality pseudotensor. (f) This vector field exhibits chirality but does not behave like a helix. As a particle is translated horizontally, it rotates about the axis into the plane. This vector field is described by an off-diagonal element of the chirality pseudotensor.

C. Chirality Pseudotensor

Chirality was first defined by Lord Kelvin as being the property where an object cannot be superimposed on its mirror image (see figure 3d). An example of such an object is a helix (see figure 3e). Indeed, chiral nematic liquid crystals derive their name from their helical director fields. In particular, helices can be either right or left handed and this is determined by the sign of the twist $\mathbf{n} \cdot \nabla \times \mathbf{n}$. However, twist fails to capture general chirality (see figure 3f). To resolve this, one can describe the chirality of a vector field \mathbf{n} using the pseudotensor

$$\chi_{ij} = \partial_i n^k \epsilon_{jkl} n^l. \quad (3)$$

This pseudotensor is defined so that the contraction $v^i \chi_{ij} u^j$ describes how the vector field \mathbf{n} rotates about the vector \mathbf{u} when displaced along the direction \mathbf{v} [36]. Thus, the diagonal terms χ_{ii} describe how the vector field rotates about the unit vector $\hat{\mathbf{e}}_i$ when moving in the direction $\hat{\mathbf{e}}_i$. That is, its trace returns the twist of \mathbf{n} .

III. Results

A. Chiral Energy

Chirality is believed to play a central role in stabilising topological solitons [14]. This would explain their presence in chiral nematic liquid crystals. The stability of these objects has previously been quantified by producing a lower bound for the free energy in terms of the Hopf charge [1]. These are celebrated results in mathematical analysis and have been realised in a number of theories [37, 38, 39, 40]. Within these theories, the energy has typically been bounded by a $\frac{3}{4}$ -exponent of the Hopf charge. This is in contrast to two dimensional Skyrmions where the energy is bounded linearly in the topological charge and therefore admits a particle-like interpretation. However, these results fail to quantify the stability of topological solitons in terms of their fundamental properties which are divorced from any field theory they may appear in.

In order to relate the chirality and the Hopf charge of the vector field, one can begin from the rational map construction described in section II A with the vector field

$$B_l = \epsilon_{ikl}\epsilon_{abc}\partial_i n^a\partial_k n^b n^c,$$

where the Einstein summation convention has been used. Indeed, this vector field has zero divergence - as required. It was shown in [37] that the Hopf charge Q satisfies

$$|Q| \leq c_0 \|B\|_1^{2/3} \|B\|_2^{4/3}, \quad (4)$$

for $c_0 \in \mathbb{R}$ a constant. This can be related to the chirality of B by observing that

$$B_l = \epsilon_{ikl}\partial_i n^a \chi_{ka},$$

where χ_{ka} is the chirality pseudotensor from (3). It follows that

$$\begin{aligned} \|B_l\|_1 &= \int \sum_{i,k,l} |\epsilon_{ikl}\partial_i n^a \chi_{ka}| \stackrel{(a)}{\leq} 3 \int \sum_{i,k} |\partial_i n^a \chi_{ka}| = 3 \int \|\partial_i n^a \chi_{ka}\|_1 \stackrel{(b)}{\leq} 3 \int \|\partial_i n^a\|_1 \|\chi_{ka}\|_1 \\ &\stackrel{(c)}{\leq} 3 \left(\int \|\partial_i n^a\|_1^2 \int \|\chi_{ka}\|_1^2 \right)^{1/2} \stackrel{(d)}{\leq} 3 \left(81 \cdot \int \|\partial_i n^a\|_2^2 \int \|\chi_{ka}\|_2^2 \right)^{1/2} = 27\sqrt{E^{(1)}E^{(2)}} \end{aligned}$$

where (a), (b), (c), (d) refer to subadditivity of the 1-norm, submultiplicativity of the entrywise matrix 1-norm, the Cauchy-Schwarz inequality for integrals, and the Cauchy-

Schwarz inequality for sums respectively. Furthermore, $E^{(1)}$ is the Dirichlet energy

$$E^{(1)} = \sum_{i=1}^3 \int |\partial_i n|^2,$$

and $E^{(2)}$ can be conceptualised as the chiral energy which may be written in a form that elucidates its relationship to the Dirichlet energy

$$E^{(2)} = \sum_{i=1}^3 \int |n \times \partial_i n|^2.$$

Applying this inequality to (4) and using the equivalence of L^1 norms yields

$$|Q| \leq c \cdot E^{(1)} E^{(2)}, \quad (5)$$

with $c \in \mathbb{R}$ a constant.

The Dirichlet energy is a measure of variability and appears as the first term of the single constant approximation to the Frank free energy. On the other hand, chiral energy is a measure of absolute chirality and unlike twist does not diminish if the vector field is both left and right handed in different directions. Thus, this result suggests that topological solitons can be stabilised by either increasing the energy of the system or by making it more chiral. In particular, since the bound does not distinguish between left and right handedness, this opens the possibility of twist reversal as a means of stabilising topological solitons as was conjectured in [14].

On top of that, a topological soliton within a purely chiral liquid crystal can be stabilised by introducing bend and splay distortions and this effect is more pronounced the greater the chirality of the material. In particular, one can bring the chirality of a topological soliton arbitrarily close to zero so long as one increases the dirichlet energy of the system by a proportional amount.

Using the calculus of variations, it can be shown that the minimisers of $E^{(1)}$ are harmonic maps satisfying

$$\sum_{i,j} \partial_i^2 n_j = 0,$$

while minimisers of $E^{(2)}$ are maps that satisfy

$$\sum_{i,j,k} \frac{1}{2} u_k (\partial_i^2 u_k - \partial_i u_j) + \partial_i u_j (\partial_i u_j - \partial_i u_k) = 0. \quad (6)$$

B. Twist Reversal

The free energy of a chiral nematic liquid crystal is minimised by a helical director with a uniform sense of twist [41]. That is, the sign of the twist $\mathbf{n} \cdot \nabla \times \mathbf{n}$ is either strictly positive or negative throughout the field. This preference for a uniform sense of twisting is also true when the liquid crystal is frustrated. Nonetheless, experimental Hopfions have been observed to violate this constraint [14].

Using the scalar map construction, the twist of the Hopf map (2) when viewed as a vector field in \mathbb{R}^3 can be expressed as

$$\mathbf{n} \cdot \nabla \times \mathbf{n} = 8 \cdot \frac{(x^2 z + y^2 z + z^3 + z)^2 - (3x^2 + 3y^2 - z^2 - 1)^2}{(x^2 + y^2 + z^2 + 1)^4}.$$

The isosurfaces of this function tile into positive and negative regions which are separated by two intersecting hyperboloids of zero twist (see figure 4a). Thus, the mathematical Hopf map exhibits twist reversal.

Chiral nematics have a preferred sense of handedness that is described by the sign of the chiral parameter q_0 in the Frank free energy (1). Hence, twist reversal results in an energetic drive to expand the region with the preferred sense of twist [41]. Consequently, the region with the opposing sense of twist contracts. This is shown for the standard $Q = 1$ Hopfion in figures 4b and 4c where the images have been obtained by means of a numerical relaxation of the Frank free energy after 1 and 3000 time steps respectively.

On the other hand, topological solitons initiate a drive towards greater chiral energy due to the canonical interpretation of (5). The trace of the chirality pseudotensor of a vector field equals its twist. Thus, the sum of the magnitudes of the off-diagonal terms of the chirality pseudotensor must increase whenever the magnitude of the twist decreases. This is seen in the isosurfaces of the diagonal chiral energy density

$$\epsilon^{(1)} = \sum_{i,j} \chi_{ij}^2 \delta_{ij}$$

and the off-diagonal chiral energy density

$$\epsilon^{(2)} = \sum_{i,j} \chi_{ij}^2 (1 - \delta_{ij})$$

shown in figures 4d and 4e respectively. Here, δ_{ij} is the Kronecker delta symbol. Indeed,

the region of minimal $\epsilon^{(1)}$ has maximal $\epsilon^{(2)}$ and the chiral energy density

$$\epsilon = \epsilon^{(1)} + \epsilon^{(2)}$$

is uniform throughout the interior of the Hopfion (see figure 4f). Together, these preferences describe the dynamics of a topological soliton as it relaxes into a stable configuration. Interestingly, the Hopfion shrinks radially but does not undergo any distortion in the winding of its preimages (see figures 4g and 4h). Furthermore, as one approaches the far field of the relaxed Hopfion, the chiral energy is minimised in a non-trivial fashion so the field configuration must approximate a solution to (6).

It has also been speculated that twist reversal helps to stabilise solitons [14]. This was justified by the observation that the Dirichlet energy is maximised around the volume of opposing twist (see figure 4i). However, the chiral energy plays a greater factor in stabilising the topological soliton and it is not clear that twist reversal is a necessary condition for the stability of these objects but rather a consequence of their geometric construction.

Materials with exotic chiral structure are of great interest because of their optical properties [36]. It is therefore important to characterise twist reversal as well as to understand whether it is a fundamental property of stable topological solitons as was argued in [14]. It can be proven that a field configuration with uniform twist and non-trivial Hopf charge must exist [41]. However, the explicit construction of such a field configuration is not yet known. In fact, there is no obvious relationship between the twist of such vector fields and the handedness of their preimages. For example, consider the negative of the rational map construction of the standard Hopf map (2). This is a topological soliton with its preimages winding with opposite handedness to that of the standard Hopf map. The twist of this vector field equals

$$\mathbf{n} \cdot \nabla \times \mathbf{n} = -8 \cdot \frac{z^2 - 1}{(x^2 + y^2 + z^2 + 1)^3}.$$

While it exhibits twist reversal at the surfaces of $z = \pm 1$, it is topologically distinct from that of its complex conjugate. It is therefore important to understand how arbitrary topological solitons are constructed and to be able to control their structure at a local scale. This is discussed in section III. C.

C. Solid Angle Construction of a $Q = 1$ Hopfion

The solid angle function can be used to construct the Hopf map using a parametric approach that considers the geometry of the desired knotted field configuration.

By definition, the preimages of any two points on S^2 under the Hopf map are a pair of linked loops on S^3 (see figure 5a). The sphere S^2 can be decomposed into a set of disjoint circles of constant latitude along with the north and south poles. The preimage of any such circle is a torus (see figure 2d). These tori continuously tile into each other (see figure 5b). We choose the preimage of the south pole to be the unit circle in the horizontal plane centered at the origin (see figure 5c). The preimage of any circle of constant latitude must be a torus that contains the preimage of the south pole within its interior. Consequently, the preimage of the north pole is fixed to be the far field and central axis (see figure 5d). While this appears to contradict the notion that the preimage of any point on S^2 must be a closed loop, the central axis can in fact be viewed as a circle through infinity [29].

We now consider the behaviour of the field in a tubular neighbourhood of the south pole preimage. On any such tubular neighbourhood, the orientation of the field must lie on a circle of constant latitude on S^2 . Furthermore, the set of points on this tubular neighbourhood that correspond to a fixed azimuthal orientation must form a closed loop. For simplicity, we consider the tubular neighbourhood that corresponds to the preimage of the equator on S^2 . This is the set of vectors in \mathbb{R}^3 that have zero z -component.

On a vertical cross section of the tubular neighbourhood, the vector field traverses all possible azimuthal orientations. That is, the vector field winds by 2π in an azimuthal direction around the preimage of the south pole (see figure 5e). This behaviour is analogous to the 4π winding of the solid angle function of a circle described in section II. B.

However, if each vertical cross section were to contain the same vector field then there would not be any linking of preimages (see figure 5g). This is resolved by twisting the tubular neighbourhood by 2π so that the preimage of a fixed orientation traces out a tilted loop (see figure 5f). Indeed, all such loops are linked with linking number 1 (see figure 5g).

We can now consider a radial neighbourhood of the preimage of the south pole. In radial directions, the azimuthal orientation must wind by π to meet the far field which corresponds with the preimage of the north pole.

To surmise, the field configuration can be parametrised using two variables α and β

which describe the field in radial and tubular directions respectively. We set

$$\alpha = \alpha(\mathbf{r}) \quad (7)$$

where \mathbf{r} is the position of a point in \mathbb{R}^3 relative to the preimage of the south pole (see figure 5i) and α satisfies the boundary conditions

$$\begin{cases} \lim_{\|\mathbf{r}\| \rightarrow 0} \alpha(\mathbf{r}) = \pi, \\ \lim_{\|\mathbf{r}\| \rightarrow \infty} \alpha(\mathbf{r}) = 0, \end{cases}$$

where ∞ represents the far field and central axis. For example, if one considers a Hopfion that is bounded in a box with side length R , then we can set

$$\alpha(\mathbf{r}) = \pi \left(1 - \frac{\|\mathbf{r}\|}{R} \right),$$

so that α indeed equals π at the preimage of the south pole and zero in the far field set to be $\|\mathbf{r}\| = R$. Next, we set

$$\beta = \frac{1}{2} \omega_K + \phi \quad (8)$$

where ω_K is the solid angle function of the preimage of the south pole and ϕ is its longitudinal phase (see figure 5i) which varies monotonically between 0 and 2π as one traverses it. Here, the solid angle function has been renormalised to exhibit the desired 2π winding. The Hopf map can then be written as

$$\mathbf{B} = \cos(\alpha) \hat{\mathbf{k}} + \sin(\alpha) \left(\cos(\beta) \hat{\mathbf{i}} + \sin(\beta) \hat{\mathbf{j}} \right). \quad (9)$$

This parametrisation clarifies the relationship between the vector field and its toroidal construction. It can also be used to initialise numerical simulations where the free energy is minimised. Indeed, we observe the construction to be stable up to homotopy after running a relaxation algorithm on the single constant Frank free energy for 3000 time steps. Furthermore, it can be used to construct other knotted field configurations by altering α and β as explored in section III. D. This is in contrast to the well established scalar map construction for which there is no direct means of constructing such fields.

D. Uniform Topological Solitons

We define a uniform topological soliton to be a field configuration where the preimages of all orientations are homotopic to each other and the preimages of any two orientations link in the same way. In particular, the standard Hopf map is an example of a uniform topological soliton since the preimage of any orientation is a closed loop and the preimages of any two orientations form a Hopf link.

D..1 Arbitrarily Knotted Preimages

A generalisation of the construction in section III. C. is to consider a field where the preimages of orientations are knots instead of loops. We restrict our discussion to tame knots which are defined as having non-zero thickness throughout the knot.

Any knot can be uniquely decomposed into a class of knots known as prime knots [42]. While there is no known method of generating all prime knots, they have been widely documented and ordered by their number of crossings. Additionally, every tame knot is either a torus, satellite, or hyperbolic knot [43]. Therefore, it is illustrative to consider knotted fields whose preimages are prime examples of each kind.

In principle, the field in (9) generalises to any knot K provided the solid angle function ω_K and longitudinal phase ϕ are recomputed for that instance of the knot. However, we further require that the level sets of the solid angle function for a given curve K be well defined and only intersect at the boundary of K . The class of knots that satisfy this property are said to be fibered. Knots that are not fibered cannot be smoothly encoded into uniformly knotted fields. Their solid angle functions feature singular regions.

A (p, q) -torus knot is constructed by winding a thread p times around the hole of a torus and q times around its outer axis before joining its two ends together. Every torus knot is fibered. A topological soliton with $(3, 2)$ -torus knotted preimages is shown in figure 6a. To ensure that the preimages do not self-intersect, the radial parameter in (7) must be chosen appropriately both in its local structure and rate of decay.

A satellite knot K is constructed from an arbitrary nontrivial knot k by embedding it inside a torus so that it links with the central axis of the torus and then tying up the torus into a nontrivial knot. Necessary and sufficient conditions for a satellite knot to be fibered are given in [44]. A topological soliton with satellite knotted preimages is shown in figure 6b.

A hyperbolic knot is a curve whose complement admits a Riemannian metric of con-

stant curvature -1 . These are the least understood class of knots and as such there is no known criteria for when they fiber. The topological soliton in figure 6c has hyperbolic knotted preimages in the shape of the figure eight knot.

The pictured PT constructions have not been relaxed so as to illustrate the geometry of the solid angle construction. Nonetheless, they were observed to be stable for 3000 time steps with very little deviation from the initial configuration.

D..2 Arbitrarily Linked Preimages

Links generalise knots to multiple components. By linearity of the scalar potential, the solid angle ω of a link L with knot components k_1, \dots, k_n is given by

$$\omega_L = \omega_{k_1} + \dots + \omega_{k_n}.$$

The longitudinal phase ϕ of a link also distributes over its components. Thus, the construction in (9) generalises to topological solitons whose preimages are arbitrary links. In particular, each knot component of the link must obey the criteria discussed in section III. D..1. Moreover, the radial parameters of individual knot components must not interfere with each other so the far field must be defined accordingly.

The simplest link is the unlink where two knots are jointly considered without being linked. This may be encoded by embedding one topological soliton in the far field of the other. In figure 6d, two Hopfions have been co-axially aligned. The preimage of an orientation is an unlink and the preimage of any two orientations is a pair of unlinked Hopf links. Thus, the Hopf invariant of this field is 2.

The next simplest link is the Hopf link. The PT construction in figure 6e is the result of computing (9) for a Hopf link. The preimage of any orientation is a Hopf link (see figure 6h) and the preimage of any two orientations is a pair of linked Hopf links (see figure 6i). However, this construction is not axially symmetric nor does it maximise the volume it is embedded within. Indeed, there are multiple ways that a Hopf link may be encoded in the nodal lines of a knotted field.

One approach is to set the tubular parameter in (9) to

$$\beta = \frac{1}{2}N\omega_K + \phi,$$

where $N = 2$ but can be any integer which equals the desired Hopf invariant of the knotted

field. The preimage of any such orientation is a Hopf link and the preimages of any two such orientations is a linked pair of Hopf links. Geometrically, the twist of each toroidal layer in the Hopfion has been doubled (see figure 6f).

Alternatively, the radial parameter in (9) can be normalised so that

$$\pi \geq \alpha \geq (1 - N)\pi,$$

where $N = 2$ fixes the Hopf invariant. Here, the preimage of any orientation is a Hopf link. However, the PT construction of the resulting field is starkly different. Geometrically, the twist in radial directions has been doubled. Topologically, one Hopfion has been nested inside another (see figure 6g).

This example demonstrates that a link may be encoded in the preimages of a field in several different ways while preserving the linking between preimages. Formally, the Hopf state characterised by Hopf linked preimages is topologically degenerate. It is therefore important to consider the global structure of a field. This has various implications for the energy of the configuration and can be exploited by technological applications of three dimensional topological solitons.

D..3 Arbitrary Linking between Preimages

The manner in which the preimages of any two orientations link determines the Hopf invariant of the knotted field. Non-Hopf linked examples have only recently been observed in [45] so it is of interest to characterise all such possible linking schemes.

Given arbitrary Hopf charge N , the tubular parameter in (8) may be set to

$$\beta = \frac{1}{2}\omega_K + N\phi,$$

so as to produce a topological soliton whose preimages are loops and any two preimages have linking number N . The precise manner in which these preimages are linked is known as a torus link since they may be fibered to fill the surface of a torus (see figures 6j, 6k, 6l). We suggest that this was the first non-Hopf linked topological soliton to be experimentally observed since it is energetically inexpensive to introduce additional winding in tubular directions. These are easily generalised to arbitrary base knots K by recomputing the solid angle function appropriately.

E. Non-Uniform Topological Solitons

The non-uniform topological solitons observed in [14, 45] have not appeared in the theoretical literature. The preimages of these solitons link differently across different regions of S^2 . This allows more information to be encoded in a smaller volume and is therefore well suited for technological applications. A theoretical description of them will offer guidance towards the construction of a wider class of these objects as well as contribute to new developments in topology and differential geometry.

E..1 Solitons with Undefined Hopf Invariant

The first non-uniform topological soliton was observed in [14]. Notably, this construction does not have a well defined Hopf charge since the preimages of different regions of S^2 link differently. For this soliton, preimages of any two orientations above some critical angle θ_c form a pair of linked Hopf links (see figure 7a). On the other hand, the preimages of any two orientations below this critical angle form a pair of unlinked Hopf links (see figure 7b). If one orientation is chosen above the critical angle and another below it, then the linking of preimages is as shown in figure 7c. These preimages can be represented as graphs for which every vertex represents a closed loop and every edge signifies the existence of a Hopf link between the two connected vertices (see figures 7d, 7e, 7f). In fact, each Hopf link has linking number ± 1 . The thicker edges signify linking number $+1$ and the thinner edges represent linking number -1 . Since liquid crystals are line fields, orientations that lie on antipodal points of S^2 are indistinguishable. This means that the physically observed preimages are represented by the graphs shown in figures 7g, 7h, 7i.

Next, we consider the global structure of this field. The preimage of the south pole of S^2 occupies two loops. The preimage of the north pole includes a loop positioned between the two north pole preimages, as well as the far field and central axis (see figure 8a). We will be considering bounded Hopfions for which the far field is confined to an outer torus.

The preimage of a circle of constant latitude below the critical angle forms a pair of co-axially aligned tori (see figure 8b). However, notice that both of these tori have been deformed and that this deformation is not purely radial as in the case discussed in section III. B. This is because the field configurations corresponding to regions below and above the critical angle must continuously tile into each other. Furthermore, the individual loop preimages on the inner torus have linking number -1 , whereas the preimages on the outer torus have linking number $+1$. This is easily seen from the fact that the colour patches

on the PT construction of the inner torus rotate with opposing handedness to those on the outer torus.

On the other hand, the preimage of a circle of constant latitude above the critical angle forms a pair of nested tori (see figure 8c). Again, these tori have been deformed and the individual loop preimages on the inner torus have linking number -1 , while those on the outer torus have linking number $+1$.

We see that this construction comprises a set of co-axially aligned or otherwise nested tori whose preimages span regions of S^2 . Thus, to construct this vector field explicitly, we must first define Hopfions whose preimages only cover a subregion of S^2 . We set

$$\mathbf{B} = \mathbf{B}(\mathbf{x}; S, \Sigma, \theta_0, \theta_1)$$

to be the field in (9) with three additional constraints. Firstly, its preimages are restricted to vary between the azimuthal orientations θ_0 and θ_1 in outward radial directions. This is achieved by adjusting β in (8). Secondly, it must be equal to θ_1 on the surface Σ and zero beyond this surface. That is, Σ defines the far field so it can be set by adjusting α in (7). Finally, S specifies the south pole preimage around which the Hopfion is constructed. These conditions are sketched in figure 8d for a Hopfion which has θ_0 and θ_1 greater than the south pole so that it is left hollow in the middle. On the other hand, figure 8e shows such a Hopfion with θ_0 equal to the south pole so that forms it a thin solid tube. Now these different fields can be summed together to yield a non-uniform topological soliton.

This construction of a non-uniform topological soliton extends to all such objects. One considers individual solitons which traverse a limited region of S^2 and then composes these solitons to form a non-uniform topological soliton.

To generalise this axisymmetric construction, we note that there are two possible operations one can perform: co-axial alignment of Hopfions (see figure 8b) and nesting of Hopfions (see figure 8c). We can represent this as a family of graphs (see figure 8f). Let each vertex on a graph represent a component of the non-uniform topological soliton. Then each directed edge indicates that the child torus is nested within the parent torus. Two vertices which are not connected by an edge must be co-axially aligned so as to maintain the planar axisymmetry of the field configuration. Then if we introduce an additional edge to the graph, this connection must also be appended to each antecedent element in the graph. That is, every directed path forms a complete graph. This characterises the set of all such possible graphs.

E..2 Solitons with Broken Axial Symmetry

Topological solitons with broken axial symmetry have also been observed. Figure 8g shows how one such topological soliton divides S^2 into asymmetric regions, each of which exhibits both a different preimage (see figure 8h) and a different linking of preimages (see figure 8i). Again, we can consider each subspace of S^2 separately and construct three different topological solitons. However, since we are no longer dealing with an axisymmetric field configuration, it is clear that these solitons are not simply co-axially aligned or nested. Instead, they wind around each other to form linked solitons. This is again easily parametrised using the solid angle function provided that the far field is chosen appropriately.

IV. Conclusion

Using recent insights into the local structure of the solid angle function as well as its numerical implementation, we have derived a parametric construction of the standard Hopf map (9) that immediately generalises to arbitrarily linked and knotted field configurations. In doing so, we have unified the theoretical description of topological solitons which have previously been studied using the rational map construction described in section II. A. Furthermore, since the solid angle function corresponds to the magnetostatic potential of a current-carrying wire, it may be possible to directly translate this parametrisation into an experimental procedure involving the motion of a lazer tweezer in a liquid crystal. This would open the possibility of automating the generation of topological solitons, resulting in immediate technological applications.

In addition to this, we have characterised non-uniform topological solitons both in terms of their linking of preimages as well as their global structure. These objects have not previously appeared in the theoretical literature and are relevant to all areas of physics where the existence of topological solitons has been stipulated. Their non-uniform structure may also lead to new developments in the fields of topology and differential geometry. Indeed, their theoretical description is made possible because of the solid angle approach and it is unclear how this might be reproduced with the rational map construction.

Most importantly, we have characterised the stability of topological solitons in terms of the chiral energy of the system (5). This justifies their prevalence in chiral nematic liquid crystals and provides guidance towards realising them in other physical systems.

The chiral energy is shown to be related to the Dirichlet energy and one may therefore assume that it will result in developments in the field of partial differential equations. Through numerical minimisation of the Frank free energy, we have shown that the chiral energy plays an important role in stabilising a Hopfion and that the manner in which it does this affects the dynamics of the Hopfion as it relaxes into a stable field configuration. Very little is known about Hopfion dynamics and this is a crucial first step that may be followed by considering how the chiral energy varies as one introduces an external potential, thereby causing the Hopfion to transition between different Hopf states.

Finally, the characterisation of point singularities and line defects was beyond the scope of our work. It is not straightforward how these may be modeled and their characterisation in terms of chiral energy is of immediate interest. In particular, it is possible to bring the two point singularities of a Toron together so that they may annihilate and form a smooth Hopfion. This effect is poorly understood and a study of its chiral energy may prove insightful.

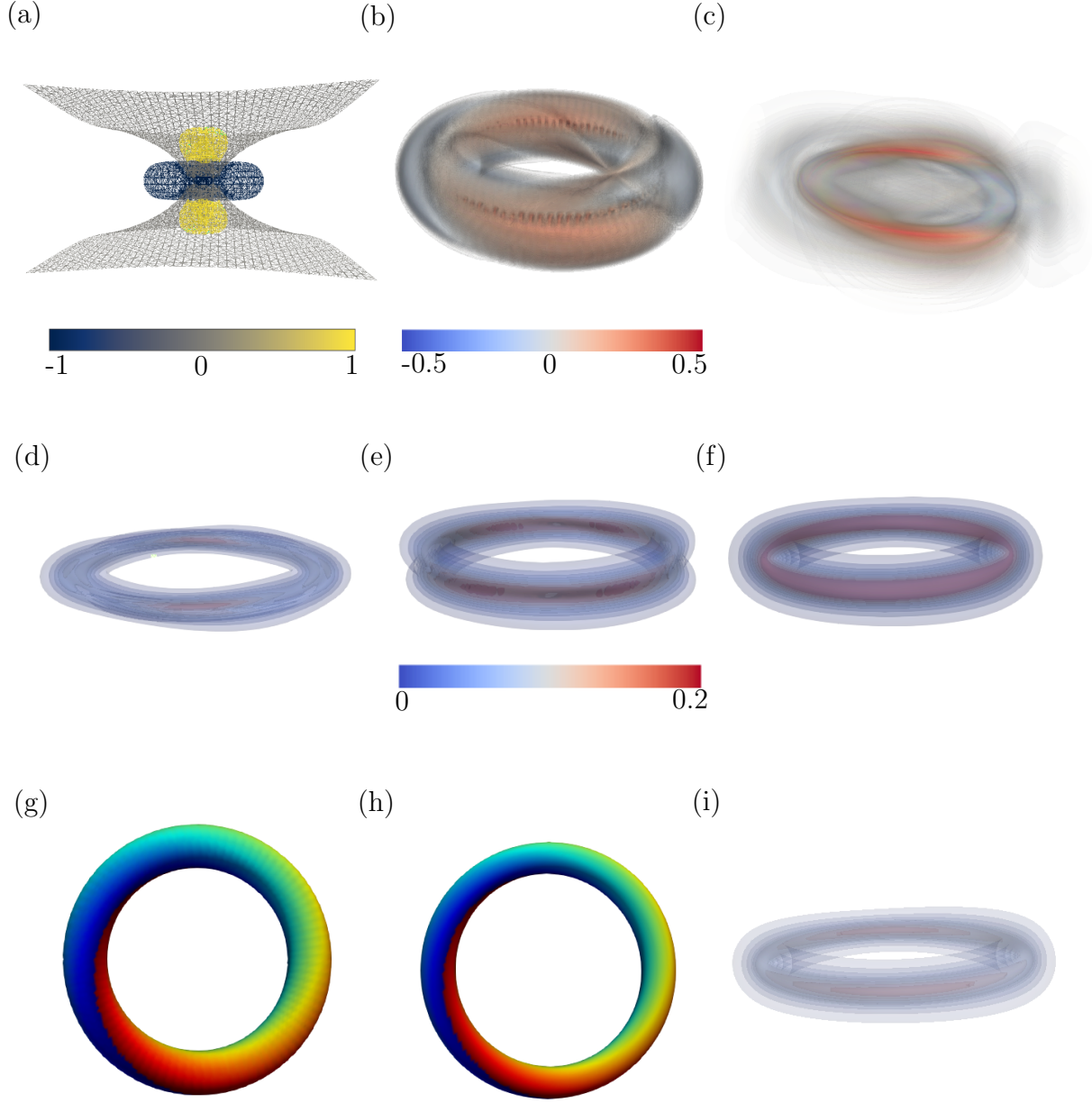


Figure 4: Twist isosurfaces of (a) the standard Hopf map, (b) a bounded Hopfion after 1 relaxation time step, and (c) a bounded Hopfion after 3000 relaxation time steps. The incorrectly handed region (red) has shrunken. The opacity of the outer regions has been reduced to show the interior. (d) Isosurfaces of the diagonal chiral energy density $\epsilon^{(1)}$ for a bounded Hopfion. (e) Isosurfaces of the off-diagonal chiral energy density $\epsilon^{(2)}$ for a bounded Hopfion. (f) Isosurfaces of the chiral energy density ϵ for a bounded Hopfion. (g) PT construction of a bounded Hopfion after 1 relaxation time step. (h) PT construction of a bounded Hopfion after 3000 relaxation time steps. It is clearly thinner than the previous image. (i) Isosurfaces of the Dirichlet energy of a bounded Hopfion. The magnitude of the Dirichlet energy never exceeds that of the chiral energy and therefore plays a lesser role in stabilising the Hopfion. However, it is maximised around the volume of opposing twist as observed in (5).

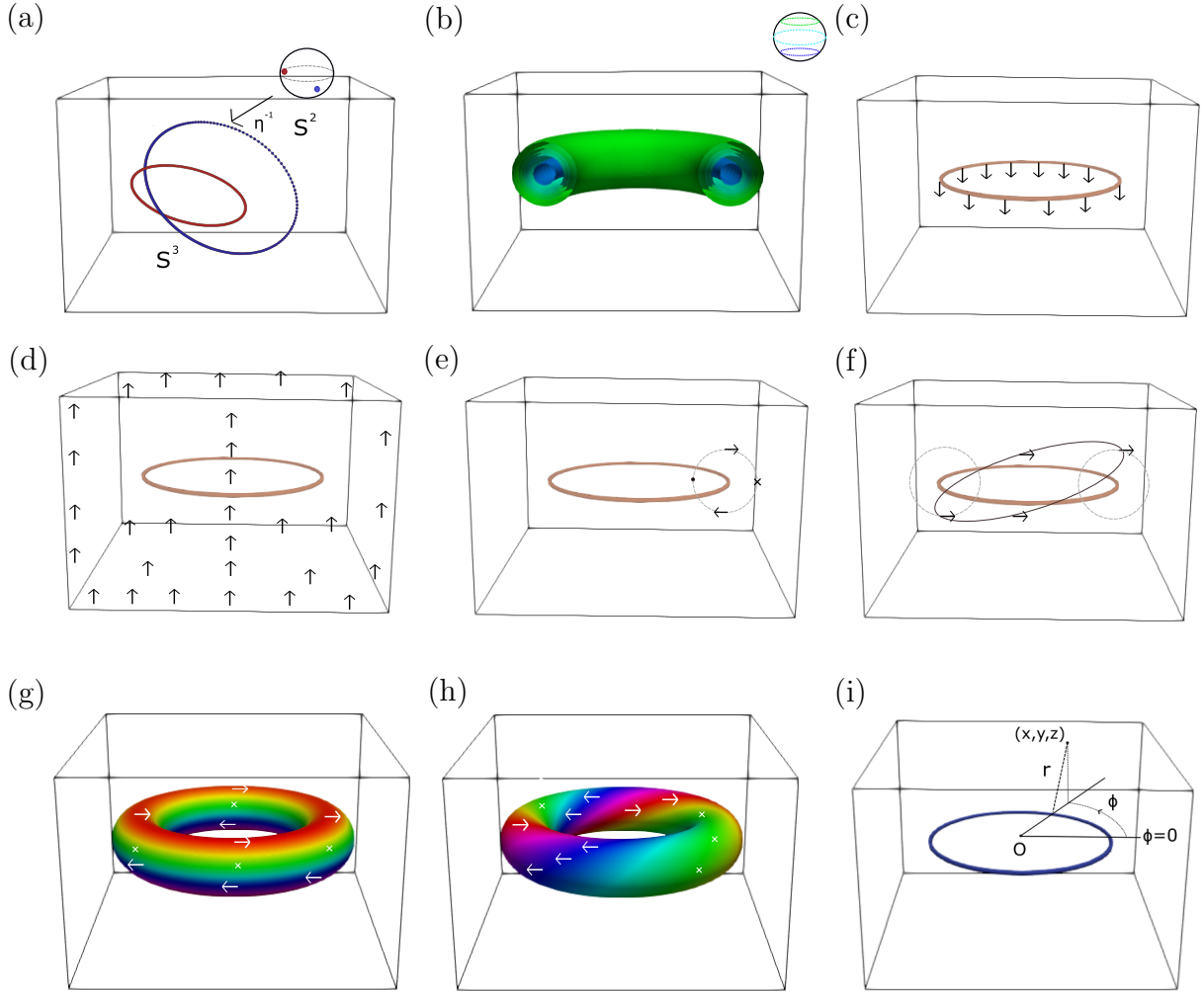


Figure 5: (a) The preimages of two distinct points on S^2 under the Hopf map form a pair of linked loops. Viewed as a vector field, the set of points in the Hopfion that are oriented along any two fixed orientations form a pair of linked loops. (b) The preimage of a circle of constant latitude on S^2 under the Hopf map forms a torus. The toroidal preimages of any such longitudinal arcs form nested tori. (c) The preimage of the south pole forms an individual loop with the vector field pointing downwards along it. (d) The preimage of the north pole lies in the far field and along the central axis. (e) A circular cross section of the Hopfion coinciding with one of the longitudinal tori must contain all azimuthal orientations. (f) Fixed orientations must wind by 2π around the vertical cross section as one traverses the torus. (g) PT construction of a vector field where the cross section does not wind as one traverses the torus. It is clear that the circles are disjoint but do not link. (h) PT construction of a vector field where the cross section winds by 2π as one traverses the torus. It can be shown that the preimages of any two orientations have linking number 1. (i) r denotes the distance between a point (x, y, z) and the closest point on the south pole preimage. ϕ denotes the longitudinal phase of the point and requires the choice of an axis denoting $\phi = 0$ which is defined to be normal to the south pole preimage.

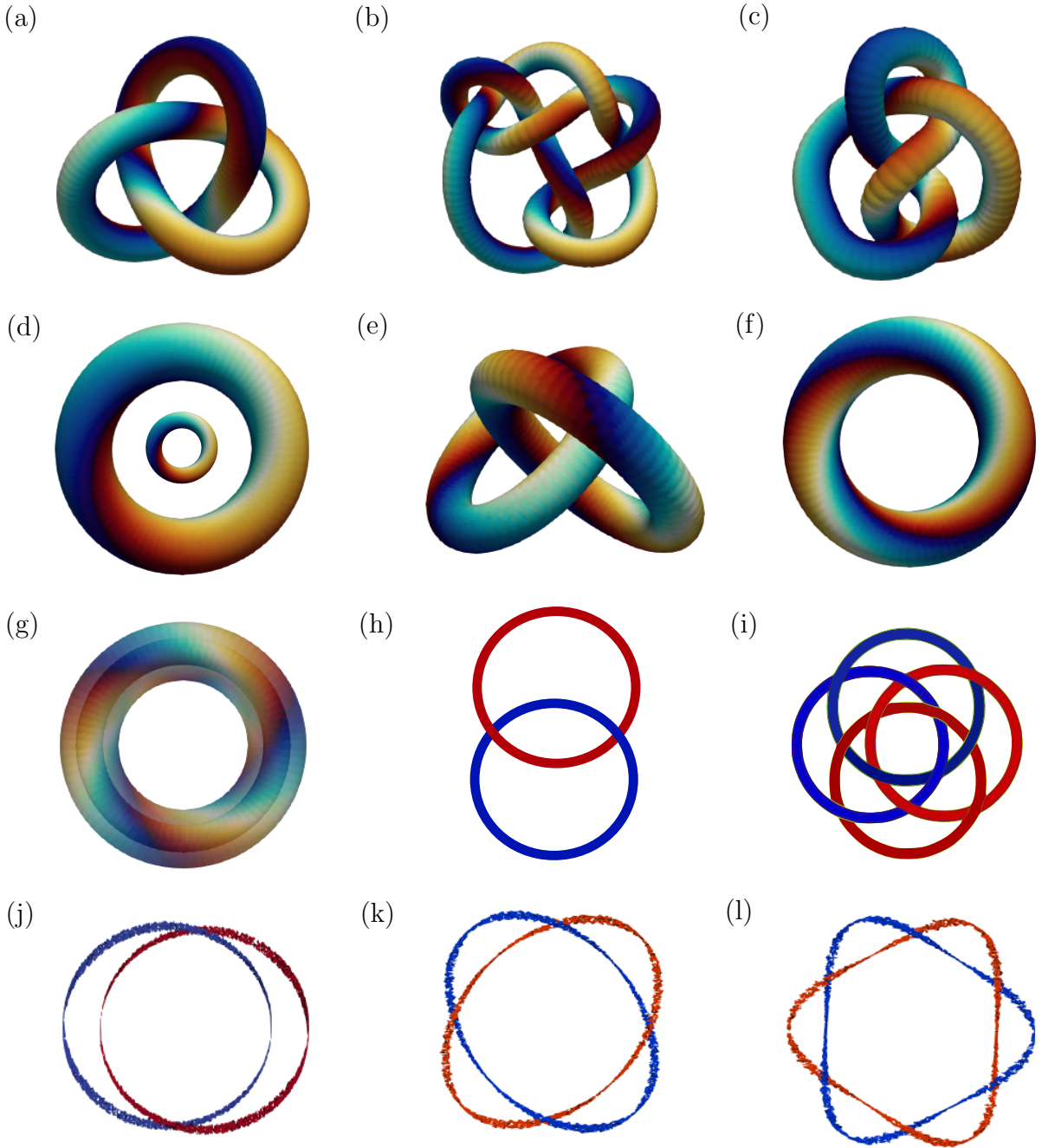
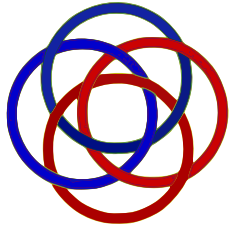
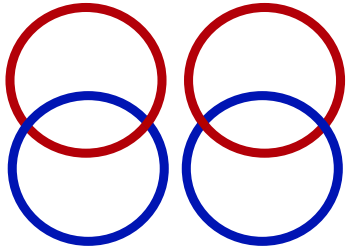


Figure 6: Unrelaxed PT constructions of uniform topological solitons with (a) torus (b) satellite and (c) hyperbolic knotted preimages respectively. (d) Co-axially aligned Hopfions. The Hopf invariant of the combined structure is $1 + 1 = 2$. The preimage of any orientation is a pair of loops. The preimage of any two orientations is a pair of Hopf links. (e) Hopf linked Hopfions. (f) Hopfion with 4π tubular twist. (g) Hopfion with 2π radial twist. The preimage of a circle of constant latitude on S^2 is a pair of nested tori. The opacity of the construction has been reduced to show this nesting. (h) The preimage of any orientation in (e), (f), (g) is a Hopf link. (i) The preimage of any two orientations in (e), (f), (g) is a pair of linked Hopf links. Every loop is Hopf linked to every other loop. The combined Hopf invariant is 2. This is seen by either summing the signed crossings between the blue and red components or by noticing that S^2 is traversed twice in each of the PT surfaces. (j) Hopf link resulting from $\phi = 2\pi$. (k) Solomon link resulting from $\phi = 4\pi$. (l) Torus link resulting from $\phi = 6\pi$.

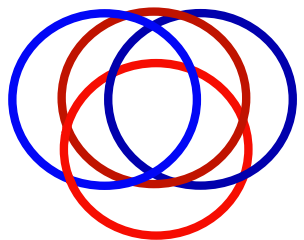
(a)



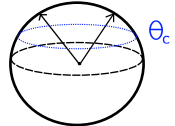
(b)



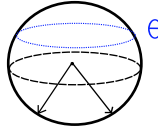
(c)



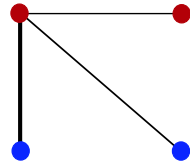
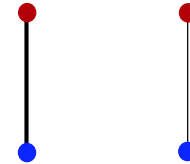
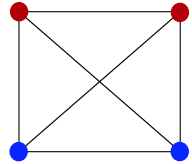
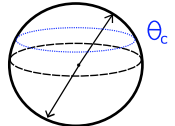
(d)



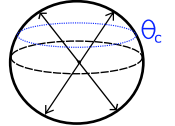
(e)



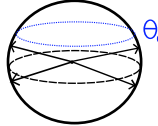
(f)



(g)



(h)



(i)

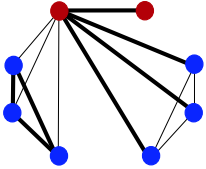
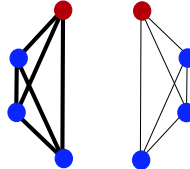
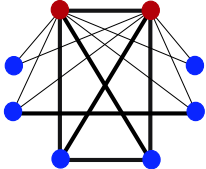
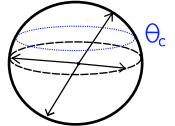


Figure 7: The linking of preimages of an observed non-uniform $Q = 2$ topological soliton (a) with both orientations above some critical angle θ_c , (b) with both orientations below θ_c , (c) with one orientation above θ_c and the other below θ_c . Graph representations of (a), (b), (c) are shown in (d), (e), (f) respectively. Graph representations of four orientations as indicated on their respective spheres are shown in figures (g), (h), (i). These preimages are particularly relevant to liquid crystals where antipodal points on a sphere are considered equivalent.

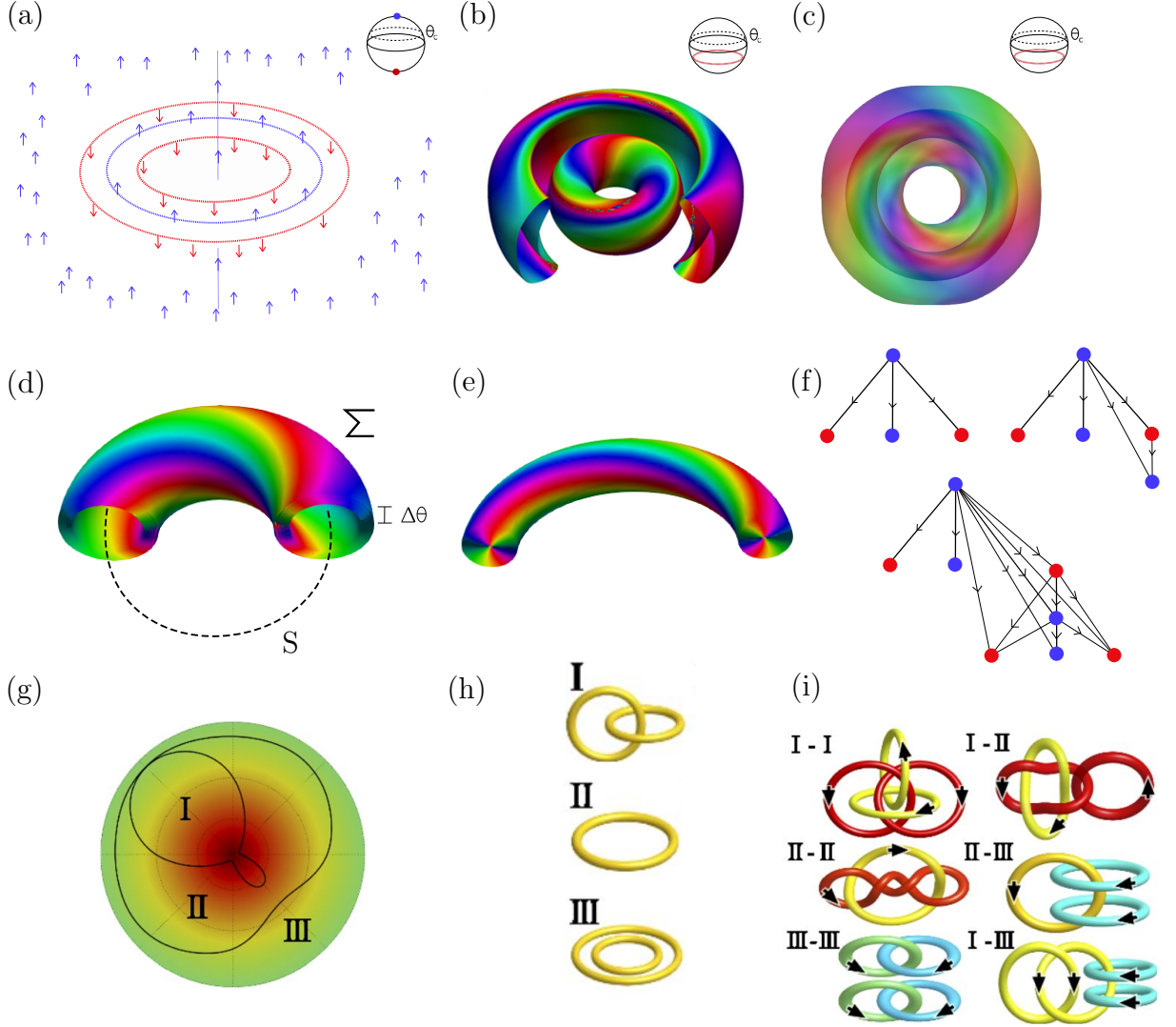


Figure 8: (a) The preimages of the north and south poles for a non-uniform topological soliton. (b) The preimage of a circle of constant latitude with azimuthal orientation strictly less than the critical angle is a pair of co-axially aligned tori. (c) The preimage of a circle of constant latitude with azimuthal orientation strictly greater than the critical angle is a pair of nested tori. (d) A topological soliton constructed around a loop S with far field Σ has its azimuthal orientation restricted so that it is hollow inside. This allows for another Hopfion to be nested inside of it. (e) A topological soliton with its azimuthal orientation restricted so that it forms a thin solid tube. (f) Graphs representing the nesting and co-axial alignment of various uniform topological solitons to form non-uniform topological solitons. Each vertex is coloured by whether the topological soliton has azimuthal orientation strictly greater than the critical angle (blue) or strictly less (red). If a new vertex is connected to a nested element in the graph, then the vertex must also be connected to that element's parent. (g) A non-uniform topological soliton divides S^2 into regions with broken axial symmetry. The orientation in each region has a preimage as shown in (h) and the linking of its preimages is shown in (i).

References

- [1] Nicholas Manton and Paul Sutcliffe. *Topological solitons*. Cambridge University Press, 2004. doi: [10.1017/CBO9780511617034](https://doi.org/10.1017/CBO9780511617034).
- [2] Lord Kelvin. On vortex atoms. *Proceedings of the Royal Society of Edinburgh*, 6:94–105, 1867. doi: [10.1017/S0370164600045430](https://doi.org/10.1017/S0370164600045430).
- [3] William TM Irvine and Dirk Bouwmeester. Linked and knotted beams of light. *Nature Physics*, 4(9):716, 2008. doi: [10.1038/nphys1056](https://doi.org/10.1038/nphys1056).
- [4] Henry Keith Moffatt. The degree of knottedness of tangled vortex lines. *Journal of Fluid Mechanics*, 35(1):117–129, 1969. doi: [10.1017/S0022112069000991](https://doi.org/10.1017/S0022112069000991).
- [5] Mitchell A Berger. Introduction to magnetic helicity. *Plasma Physics and Controlled Fusion*, 41(12B):B167, 1999. doi: [10.1088/0741-3335/41/12B/312](https://doi.org/10.1088/0741-3335/41/12B/312).
- [6] Amy Thompson, Alexander Wickes, Joe Swearngin, and Dirk Bouwmeester. Classification of electromagnetic and gravitational hopfions by algebraic type. *Journal of Physics A: Mathematical and Theoretical*, 48(20):205202, 2015. doi: [10.1088/1751-8113/48/20/205202](https://doi.org/10.1088/1751-8113/48/20/205202).
- [7] Stephen C Davis, Anne-Christine Davis, and Mark Trodden. $N = 1$ supersymmetric cosmic strings. *Physics Letters B*, 405(3-4):257–264, 1997. doi: [10.1016/S0370-2693\(97\)00642-4](https://doi.org/10.1016/S0370-2693(97)00642-4).
- [8] Jan Seidel. Nanoelectronics based on topological structures. *Nature materials*, 18(3):188, 2019. doi: [10.1038/s41563-019-0301-z](https://doi.org/10.1038/s41563-019-0301-z).
- [9] H Yoshida, K Asakura, Junichi Fukuda, and M Ozaki. Three-dimensional positioning and control of colloidal objects utilizing engineered liquid crystalline defect networks. *Nature communications*, 6:7180, 2015. doi: [10.1038/ncomms8180](https://doi.org/10.1038/ncomms8180).
- [10] Apala Majumdar, CJP Newton, JM Robbins, and M Zyskin. Topology and bistability in liquid crystal devices. *Physical Review E*, 75(5):051703, 2007. doi: [10.1103/PhysRevE.75.051703](https://doi.org/10.1103/PhysRevE.75.051703).
- [11] Rachel Won. Liquid crystals: Realizing 3d topological solitons. *Nature Photonics*, 11(5):273, 2017. doi: [10.1038/nphoton.2017.66](https://doi.org/10.1038/nphoton.2017.66).

- [12] Ran Cheng, Maxwell Li, Arjun Sapkota, Anish Rai, Ashok Pokhrel, Tim Mewes, Claudia Mewes, Di Xiao, Marc De Graef, and Vincent Sokalski. Magnetic domain wall skyrmions. *Physical Review B*, 99(18):184412, 2019. doi: [10.1103/PhysRevB.99.184412](https://doi.org/10.1103/PhysRevB.99.184412).
- [13] Allen Hatcher. *Algebraic topology*. Cambridge University Press, Cambridge, 2000. doi: [10.1017/S0013091503214620](https://doi.org/10.1017/S0013091503214620).
- [14] Paul J Ackerman and Ivan I Smalyukh. Diversity of knot solitons in liquid crystals manifested by linking of preimages in torons and hopfions. *Physical Review X*, 7(1):011006, 2017. doi: [10.1103/PhysRevX.7.011006](https://doi.org/10.1103/PhysRevX.7.011006).
- [15] HK Urbantke. The hopf fibration—seven times in physics. *Journal of geometry and physics*, 46(2):125–150, 2003. doi: [10.1016/S0393-0440\(02\)00121-3](https://doi.org/10.1016/S0393-0440(02)00121-3).
- [16] Richard A Battye and Paul M Sutcliffe. Knots as stable soliton solutions in a three-dimensional classical field theory. *Physical Review Letters*, 81(22):4798, 1998. doi: [10.1103/PhysRevLett.81.4798](https://doi.org/10.1103/PhysRevLett.81.4798).
- [17] Bryan Gin-ge Chen, Paul J Ackerman, Gareth P Alexander, Randall D Kamien, and Ivan I Smalyukh. Generating the hopf fibration experimentally in nematic liquid crystals. *Physical review letters*, 110(23):237801, 2013. doi: [10.1103/PhysRevLett.110.237801](https://doi.org/10.1103/PhysRevLett.110.237801).
- [18] Jung-Shen B Tai and Ivan I Smalyukh. Three-dimensional crystals of adaptive knots. *Science*, 365(6460):1449–1453, 2019. doi: [10.1126/science.aay1638](https://doi.org/10.1126/science.aay1638).
- [19] Simon Čopar and Slobodan Žumer. Nematic braids: topological invariants and rewiring of disclinations. *Physical review letters*, 106(17):177801, 2011. doi: [10.1103/PhysRevLett.106.177801](https://doi.org/10.1103/PhysRevLett.106.177801).
- [20] Bryan Gin-ge Chen, Gareth P Alexander, and Randall D Kamien. Symmetry breaking in smectics and surface models of their singularities. *Proceedings of the National Academy of Sciences*, 106(37):15577–15582, 2009. doi: [10.1073/pnas.0905242106](https://doi.org/10.1073/pnas.0905242106).
- [21] Pierre-Gilles De Gennes and Jacques Prost. *The physics of liquid crystals*, volume 83. Oxford university press, 1993.
- [22] Stefano S Turzi. On the cartesian definition of orientational order parameters. *Journal of Mathematical Physics*, 52(5):053517, 2011. doi: [10.1063/1.3589961](https://doi.org/10.1063/1.3589961).

- [23] Masao Doi. *Soft matter physics*. Oxford University Press, 2013. doi: [10.1093/acprof:oso/9780199652952.001.0001](https://doi.org/10.1093/acprof:oso/9780199652952.001.0001).
- [24] Ingo Dierking. *Textures of liquid crystals*. John Wiley & Sons, 2003. doi: [10.1002/3527602054](https://doi.org/10.1002/3527602054).
- [25] Philip W Benzie and Steve J Elston. Optics of liquid crystals and liquid crystal displays. *Handbook of Visual Display Technology*, pages 1365–1385, 2012. doi: [10.1007/978-3-540-79567-4_85](https://doi.org/10.1007/978-3-540-79567-4_85).
- [26] IA Ovidko and AE Romanov. Topological excitations (defects, solitons, textures, frustrations) in condensed media. *physica status solidi (a)*, 104(1):13–45, 1987. doi: [10.1002/pssa.2211040102](https://doi.org/10.1002/pssa.2211040102).
- [27] Sanju Gupta and Avadh Saxena. *The Role of Topology in Materials*, volume 189. Springer, 2018. doi: [10.1007/978-3-319-76596-9](https://doi.org/10.1007/978-3-319-76596-9).
- [28] John Milnor and David W Weaver. *Topology from the differentiable viewpoint*. Princeton university press, 1997.
- [29] David W Lyons. An elementary introduction to the hopf fibration. *Mathematics magazine*, 76(2):87–98, 2003. doi: [10.1080/0025570X.2003.11953158](https://doi.org/10.1080/0025570X.2003.11953158).
- [30] John Milnor. Link groups. *Ann. of Math*, 59(2):177–195, 1954.
- [31] Hridesh Kedia, David Foster, Mark R Dennis, and William TM Irvine. Weaving knotted vector fields with tunable helicity. *Physical review letters*, 117(27):274501, 2016. doi: [10.1103/PhysRevLett.117.274501](https://doi.org/10.1103/PhysRevLett.117.274501).
- [32] Raoul Bott and Loring W Tu. *Differential forms in algebraic topology*, volume 82. Springer Science & Business Media, 2013.
- [33] Harley Flanders. *Differential Forms with Applications to the Physical Sciences by Harley Flanders*, volume 11. Elsevier, 1963.
- [34] Jack Binysh and Gareth P Alexander. Maxwell’s theory of solid angle and the construction of knotted fields. *Journal of Physics A: Mathematical and Theoretical*, 51(38):385202, 2018. doi: [10.1088/1751-8121/aad8c6](https://doi.org/10.1088/1751-8121/aad8c6).
- [35] James Clerk Maxwell. *A Treatise on Electricity and Magnetism*, volume 2 of *Cambridge Library Collection - Physical Sciences*. Cambridge University Press, 2010.

- [36] Efi Efrati and William TM Irvine. Orientation-dependent handedness and chiral design. *Physical Review X*, 4(1):011003, 2014.
- [37] A. F. Vakulenko and L. V. Kapitanski. Stability of solitons in the S^2 nonlinear σ -model. *Reports of the USSR Academy of Sciences*, 246(4):840–842, 1979.
- [38] Derek Harland. Topological energy bounds for frustrated magnets. *Physical Review B*, 99(21):214405, 2019. doi: [10.1103/PhysRevB.99.214405](https://doi.org/10.1103/PhysRevB.99.214405).
- [39] Luiz Agostinho Ferreira, Nobuyuki Sawado, and Kouichi Toda. Static hopfions in the extended skyrme-faddeev model. *Journal of High Energy Physics*, 2009(11):124, 2009. doi: [10.1088/1126-6708/2009/11/124](https://doi.org/10.1088/1126-6708/2009/11/124).
- [40] Derek Harland. Topological energy bounds for the skyrme and faddeev models with massive pions. *Physics Letters B*, 728:518–523, 2014. doi: [10.1016/j.physletb.2013.11.062](https://doi.org/10.1016/j.physletb.2013.11.062).
- [41] Joseph Pollard, Gregor Posnjak, Simon Čopar, Igor Muševič, and Gareth P Alexander. Point defects, topological chirality, and singularity theory in cholesteric liquid-crystal droplets. *Physical Review X*, 9(2):021004, 2019.
- [42] H Schubert. Sitzungsber. *Heidelberger Akad. Wiss., Math.-Naturwiss. Klasse, 3rd Abhandlung*, 1949.
- [43] Colin Conrad Adams. *The knot book: an elementary introduction to the mathematical theory of knots*. American Mathematical Soc., 2004.
- [44] Mikami Hirasawa, Kunio Murasugi, Daniel S Silver, et al. When does a satellite knot fiber? *Hiroshima Mathematical Journal*, 38(3):411–423, 2008.
- [45] Jung-Shen B Tai, Paul J Ackerman, and Ivan I Smalyukh. Topological transformations of hopf solitons in chiral ferromagnets and liquid crystals. *Proceedings of the National Academy of Sciences*, 115(5):921–926, 2018. doi: [10.1073/pnas.1716887115](https://doi.org/10.1073/pnas.1716887115).